https://doi.org/10.46813/2022-137-076

UDC 621.789

EFFECT OF AUSFORMING ON MECHANICAL PROPERTIES OF 12%Cr FERRITIC/MARTENSITIC STEEL

I.F. Kislyak, H.Yu. Rostova, N.F. Andrievskaya, A.S. Kalchenko, V.S. Okovit, M.A. Tikhonovsky, R.L. Vasilenko, I.G. Tantsiura, V.A. Panov
National Science Center "Kharkov Institute of Physics and Technology", Kharkiv, Ukraine
E-mail: kislyak@kipt.kharkov.ua

Effects of ausforming through upsetting at 890 °C and following tempering on microstructure and mechanical properties under uniaxial tension of 12CrWMoNbVB ferritic/martensitic steel are studied. Electron microscopic investigations along with elemental analysis of the steel samples in various states provided detailed information about subgrain structure and typical precipitates, the latter mainly $M_{23}C_6$ and NbC carbides. Strength and plasticity parameters (σ_0, σ_b, δ) are examined and shown to enhance under applied thermomechanical treatment as compared to standard characteristics of the steel. Preferred treatment of the steel is preliminarily evaluated.

INTRODUCTION

Heat-resistant 9…12%Cr steels of the ferritic/martensitic class are promising structural materials for cores and vessel internals of new generation nuclear and thermonuclear power reactors [1–8]. However, the operating temperature range limits the use of steels of this class. On the one hand, they have a tendency to low-temperature embrittlement under radiation exposure, and on the other hand, they have a low value of heat resistance at a level of ~ 500 °C [1, 3, 8].

To increase the thermal stability of these steels with the aim of their further use in the power industry, it is necessary to increase their heat resistance and simultaneously reduce the temperatures of low-temperature embrittlement (brittle-ductile transition) [4, 9, 10]. The main way to solve the low thermal resistance is to select the modes of thermomechanical treatments (TMT) in order to create more stable structure/phase states and improved properties in ferritic/martensitic steels. This will provide favorable conditions for the operation of the planned nuclear and thermonuclear power reactors.

One of the simple, from a technological point of view, TMT methods is high-temperature thermomechanical treatment (HTMT), which in the English literature is called ausforming. HTMT or ausforming is the heating of steel to temperatures of stability of austenite, deformation at these temperatures (or temperatures of austenite metastability) and subsequent quenching for martensite.

According to [11], ausforming in high-strength steels leads to significant hardening of martensite. Thus, the study of steel with 13%Cr and 0.3%C showed that ausforming leads to changes in the tempering stage of martensite and promotes the precipitation of fine carbides [12].

It was shown in [13] that HTMT of reactor steel EK-181 leads to a significant increase in the dislocation density in the martensite structure, as well as to an increase in the dispersity and volume fraction of vanadium carbonitride nanoparticles, which nucleate directly during deformation in the temperature range of the existence of austenite and subsequent quenching.

These processes provide a significant (by ≈ 300 MPa) increase in the values of the yield strength of steel at room temperature. Subsequent tempering at T = 720 °C (for 1 h) after HTMT also leads to a significant (compared to standard heat treatment (HT)) increase in the values of the yield strength of steel both at room temperature (by $\Delta\sigma_{0.1} \leq 290$ MPa), and at elevated temperature (T = 650 °C, by $\Delta\sigma_{0.1} \leq 100$ MPa). In this case, the plasticity remains at a fairly high level ($\delta \approx 10…13\%$) [13].

It was shown in [14] for steel Grade 91 (T91) that at room and at elevated test temperatures after HTMT, an increase in short-term mechanical properties is observed. So, after HTMT, the value of the yield strength of steel at 20 °C is 931 MPa (in the original steel it was 520 MPa), and at 550 °C it is 564 MPa (in the original steel it was 390 MPa). In this case, the width of the martensite laths after HTMT is signify-cantly smaller than after standard HT, and the sizes of $M_{23}C_6$ carbides after ausforming are comparable to their sizes after standard HT, while the sizes of MX carbides (carbonitrides) are much smaller.

In this regard, in a number of works [12, 15–17], it is proposed to use thermomechanical treatment in relation to 9…12%Cr ferritic/martensitic steels to increase their high-temperature strength.

In this work, we investigated a steel of this class, 12CrWMoNbVB (EI993), which is used for the manufacture of products operating at temperatures up to 620 °C [18, 19]. To increase its strength characteristics, the ausforming method was used, and a comprehensive study of the effect of HTMT on the microstructure and mechanical properties of the 12CrWMoNbVB steel was carried out.

1. MATERIALS AND METHODS

Industrial steel 12CrWMoNbVB was used as a starting material. Steel compositions according to GOST 5632-72 and according to our measurements are given in Table 1. As one can see, in contrast to the standard content of elements in this steel, there are traces of aluminum, cobalt, arsenic and a noticeable content of nickel in our sample.

Table 1

Content of elements in the test steel

Symbol	Element	Composition according to GOST 5632-72, wt.%	Our measurements, wt.%
B	Boron	Up to 0.003	0.002
C	Carbon	0.15…0.22	0.205
N	Nitrogen	–	–
Al	Aluminum	–	0.029
Si	Silicon	Up to 0.5	0.244
P	Phosphorus	Up to 0.03	0.033
S	Sulfur	Up to 0.025	0.0075
V	Vanadium	0.15…0.30	0.18
Cr	Chromium	11.0…13.0	11.69
Mn	Manganese	Up to 0.5	0.21
Fe	Iron	rest	rest
Ni	Nickel	–	0.59
Co	Cobalt	–	0.043
Cu	Copper	Up to 0.3	0.077
As	Arsenic	–	0.0035
Nb	Niobium	0.2…0.4	0.24
Mo	Molybdenum	0.4…0.6	0.42
W	Tungsten	0.4…0.7	0.38

A cylindrical steel specimen Ø 20 mm was heated in a vacuum chamber to a temperature of 1250 °C and held for 10 min, and then cooled with the camera. After that, the sample was subjected to ausforming. This treatment included heating in air to ~ 890 °C, holding at this temperature for 15 min, and following upsetting to Ø 29 mm. The degree of true deformation of the steel was $e = \ln(S/S_0) \approx 0.7$ (S_0 is the initial and S is the final cross section of the sample).

By the electroerosion method, parallel to the axis of the cylindrical billets of the initial steel and steel after ausforming, specimens in the form of dog bone were cut for testing under uniaxial tension. After that, the samples were mechanically ground and polished. The dimensions of the working area of the samples ready for testing were ≈ 0.5×1.0×5.7 mm. The samples from the ausformed steel were studied both in the initial state and after tempering. This treatment was carried out in an argon atmosphere at three modes: 720 °C for 3 h; 665 °C for 3 h; 550 °C for 25 h, with further cooling of the samples in the air.

Uniaxial tensile tests were carried out on a tensile testing machine equipped with a vacuum camera and a furnace for heating the objects under study. The samples were stretched at an average strain rate of $1 \cdot 10^{-3}$ s^{-1} at four temperatures: -196 (in liquid nitrogen); 20; 550, and 650 °C (the last two tests were carried out in vacuum). The microhardness of the samples was studied using a PMT-3 microhardness tester with a load on the indenter of 2 N, the holding time was 15 s.

Microstructural studies were carried out on an Olympus GX51 metallographic microscope and a JSM 7001F scanning electron microscope equipped with an INCA ENERGY 350 X-ray spectrum analyzer. The fine structure of the samples was studied using a JEM-2100 transmission electron microscope (TEM) (accelerating voltage 200 kV) equipped with a STEM JEOL EM-24511 scanning attachment and a JEOL EX-24063 JGP energy-dispersive X-ray microanalyzer. Samples for TEM studies were prepared by standard jet electropolishing on a Tenupol installation in an electrolyte containing 800 ml of C_2H_5OH, 100 ml of $HClO_4$, 100 ml of $C_3H_8O_3$, and a voltage of 40 V at room temperature. Parameters of subgrain structure and carbide precipitates (average subgrain sizes; size, volume fraction, and density of carbides) were determined by computer processing of microstructure images and subsequent data calculation in the ImageJ program.

2. RESULTS AND DISCUSSION

2.1. STRUCTURE

In the course of research, it was found that the strength characteristics of the initial steel, as delivered, significantly differ from the reference ones [20, 21]: σ_0 values are lower than the reference ones by 40% or more, σ_b values, too, lower by ≥ 20%. On the contrary, the δ values exceed the reference values by 8% or more, up to ~ 70%. In this regard, it was decided to perform heat treatment of the steel in order to bring it to a standard state [19, 21], namely, to process it according to the following scheme: quenching in oil from 1050 °C (15 min), subsequent tempering at 720 °C, for 3 h, and air cooling. This material and samples from it are hereinafter referred to as EI993+TT, or standard. Subsequent tests have confirmed the correctness of this approach, which will be discussed later.

The structure of a standard sample is tempered martensite with an average transverse lath size of 220 nm and is shown in Fig. 1.

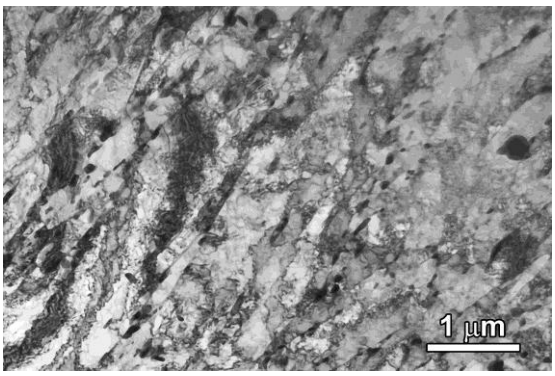

Fig. 1. The 12CrWMoNbVB steel structure in the standard state

After upsetting at temperature of 890 °C with the true deformation of 0.7, a banding microstructure with a pronounced direction of deformation and a transverse size of subgrains of 260 nm is observed (Fig. 2,a). In some areas, there is no clearly pronounced direction, the grains are oriented chaotically (see Fig. 2,b).

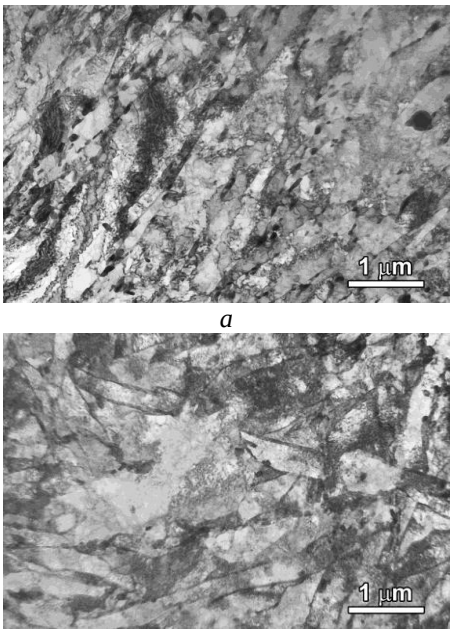

a

b

Fig. 2. The 12CrWMoNbVB steel structure after ausforming

The structure of steel samples after ausforming and subsequent tempering at three temperatures is shown in Fig. 3.

In all three modes of heat treatment, a subgrain structure with an initial stage of recrystallization is observed, when, along with the formed larger grains with clear boundaries, practically without dislocations in the grain field, there are also subgrains of the initial state 5–7 times smaller in size. There are noticeably more areas with a smaller subgrain after tempering at 550 °C for 25 h than after tempering at 720 °C for 3 h (Fig. 4). This structure can be called bimodal.

In electron microscopic images with a fine subgrain structure, dark particles are visible, located mainly along the boundaries of subgrains and lamellas (see Fig. 3). Some of them are hardly detected due to the increased density of subgrain boundaries and dislocations. These particles are more clearly visible when examining the samples in an electron microscope in the STEM mode (see Fig. 4).

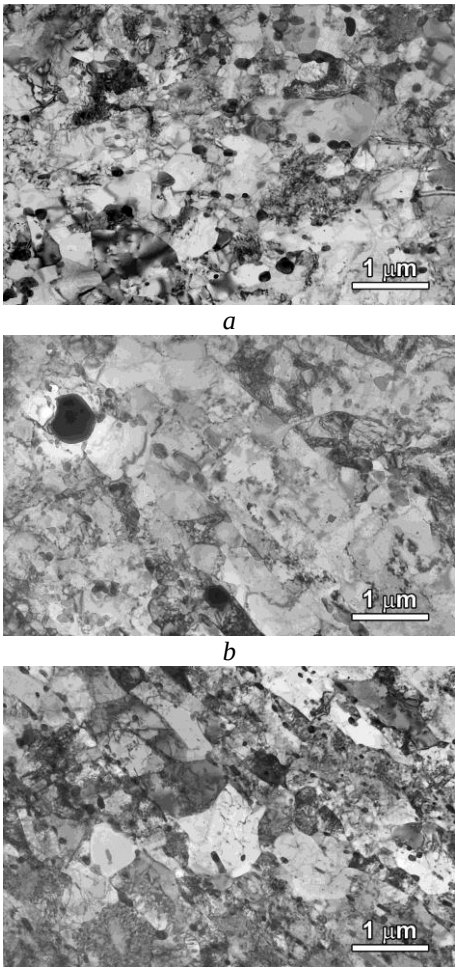

a

b

c

Fig. 3. TEM-structure of the 12CrWMoNbVB steel after ausforming and subsequent temperings at 720 °C for 3 h (a); 665 °C for 3 h (b); 550 °C for 25 h (c)

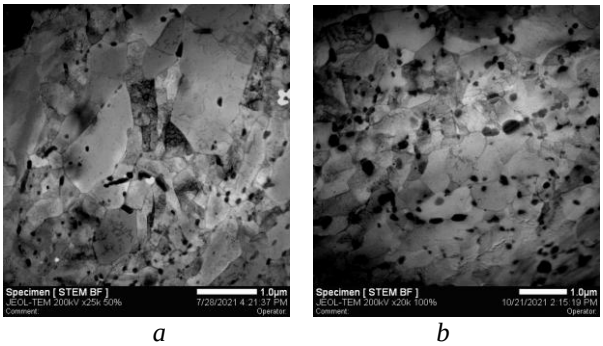

a *b*

Fig. 4. STEM-images of the samples after ausforming and subsequent temperings at 720 °C for 3 h (a) and 550 °C for 25 h (b)

On the basis of computer processing of microstructure images and data calculation in the ImageJ program, the structural characteristics of steel samples in various states are determined. The obtained data are summarized in Table 2. An energy-dispersive X-ray microanalyzer was used to precisely study the composition of the particles. Fig. 5 shows an image of a

section of a standard sample with one large dark particle and many smaller ones.

Analysis of a large dark precipitate (Table 3, No. 1) revealed that it consists mainly of niobium and a small along the boundaries of subgrains and lamellas (see Fig. 3). Some of them are hardly detected due to the increased density of subgrain boundaries and dislocations. These particles are more clearly visible when examining the samples in an electron microscope in the STEM mode (see Fig. 4).

Table 2

Structural characteristics of steel samples in various states

State		EI993+TT	Subsetting+ tempering at 720 °C for 3 h	Subsetting+ tempering at 665 °C for 3 h	Subsetting+ tempering at 550 °C for 25 h
$M_{23}C_6$	ρ, m^{-3}	$7.2 \cdot 10^{19}$	$4 \cdot 10^{19}$	$5.5 \cdot 10^{19}$	$8.8 \cdot 10^{19}$
	d, nm	100	128	141	86
	V, %	3.6	3.8	6.0	3.5
NbC	ρ, m^{-3}	$1.8 \cdot 10^{18}$	$3.5 \cdot 10^{17}$	$9 \cdot 10^{17}$	–
	d, nm	343	385	506	–
	V, %	1.5	0.3	0.2	–
Average size of subgrains and lamellae, nm		220	310	290	305

Fig. 5. Carbide precipitates in the standard sample

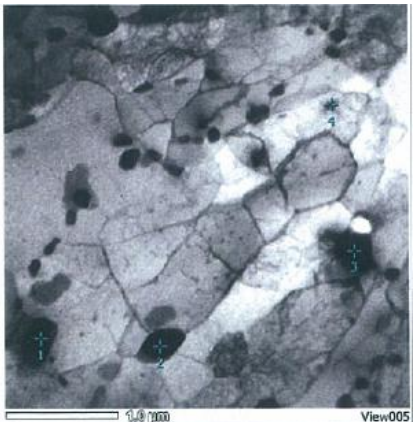

Fig. 6. STEM-image of a sample after tempering at 720 °C for 3 h

Table 3

Elemental composition of precipitates in the standard sample (see Fig. 5)

No.	at.%								
	C	Si	V	Cr	Mn	Fe	Nb	Mo	W
1	13.03	0.24	0.42	14.67	0.36	13.82	51.16	6.27	0.03
2	17.45	0.00	0.00	53.58	1.43	23.77	0.00	2.34	1.42
No	wt.%								
	C	Si	V	Cr	Mn	Fe	Nb	Mo	W
1	2.20	0.09	0.30	10.75	0.28	10.87	66.95	8.47	0.08
2	4.29	0.00	0.00	57.00	1.61	27.16	0.00	4.59	5.35

Analysis of a large dark precipitate (see Table 3, No. 1) revealed that it consists mainly of niobium and a small amount of chromium and molybdenum, while small ones (see Table 3, No. 2) are composed of chromium, iron, traces of manganese, molybdenum, and tungsten. Fig. 6 gives a view of a sample area after tempering at 720 °C for 3 h, and Table 4 shows the elemental composition of individual particles (No. 1–3) and matrix (No. 4). The particles show an increased content of chromium, iron, the presence of manganese, molybdenum and tungsten, which is typical for $M_{23}C_6$ carbides. The presence of all alloy elements with predominance of iron, low chromium content, but with out manganese and tungsten is determined in the matrix. Chromium, manganese, and tungsten actively interact with carbon to form carbides.

In scanning mode, cartograms were taken from some areas of the studied samples. Fig. 7 shows a cartogram of a sample area after tempering at 665 °C for 3 h. Chromium, iron, molybdenum are concentrated in small particles, and a significant part of the large particle is niobium with the presence of molybdenum, vanadium, and tungsten. In this case, carbon is not determined unambiguously due to its low atomic weight. Electron diffraction patterns confirm that large particles are carbides of the MC type, where, in our case, niobium is the predominant M-element, and small particles are carbides of the $M_{23}C_6$ type.

Table 4

Elemental composition of precipitates in a sample after tempering at 720 °C for 3 h (see Fig. 6)

No.	at.%								
	C	Si	V	Cr	Mn	Fe	Nb	Mo	W
1	40.53	0.83	0.00	36.39	1.80	16.64	0.69	2.27	0.84
2	32.90	0.00	0.00	41.07	1.18	22.48	0.00	1.82	0.55
3	22.91	0.00	0.48	30.21	0.00	45.29	0.00	0.71	0.40
4	28.62	0.60	0.86	11.05	0.00	56.38	0.98	1.48	0.04
No.	wt.%								
	C	Si	V	Cr	Mn	Fe	Nb	Mo	W
1	12.59	0.61	0.00	48.93	2.56	24.03	1.65	5.64	4.00
2	9.57	0.00	0.00	51.75	1.56	30.42	0.00	4.23	2.46
3	6.06	0.00	0.54	34.59	0.00	55.69	0.00	1.50	1.62
4	7.87	0.38	1.00	13.16	0.00	72.10	2.09	3.24	0.15

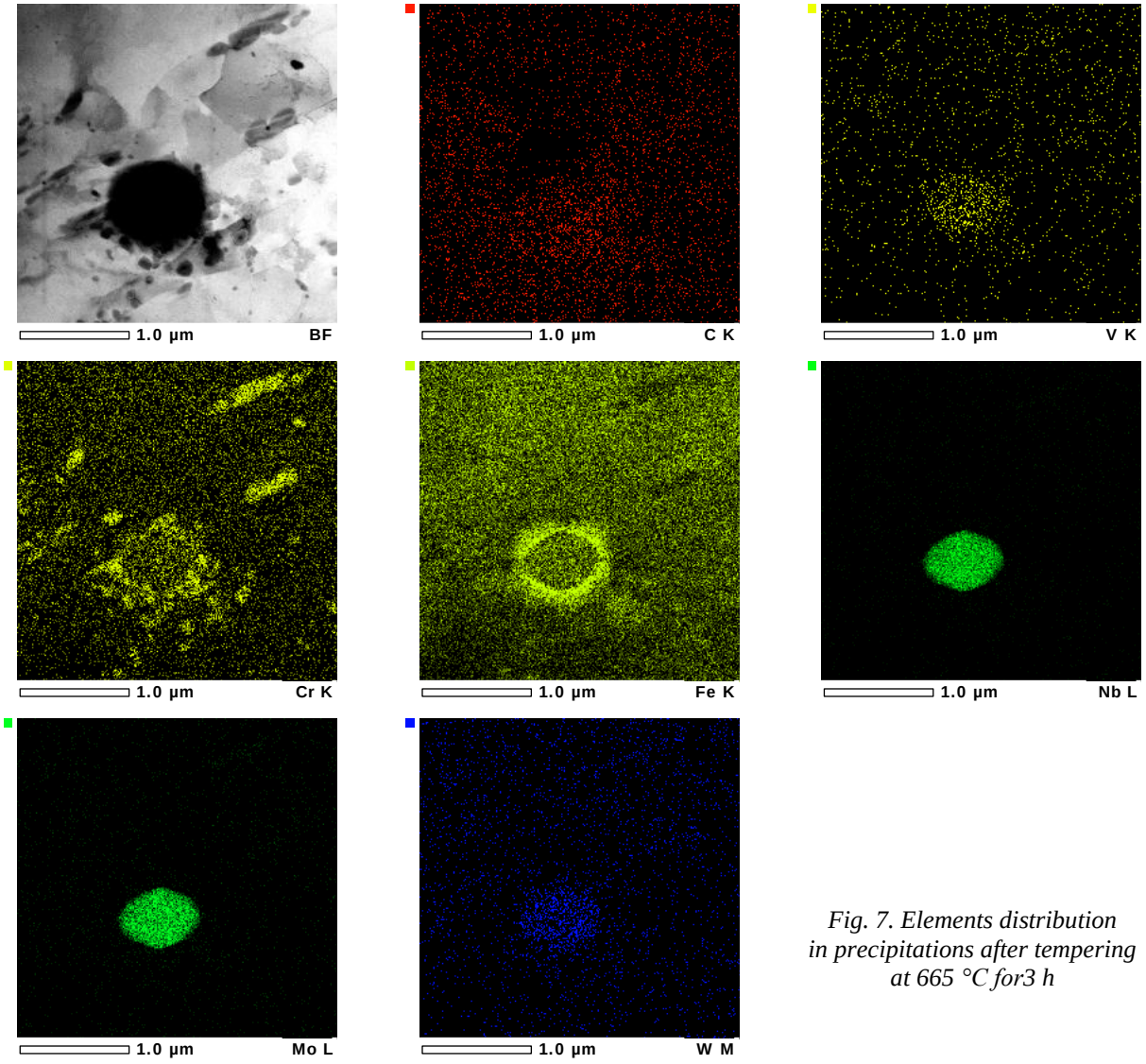

Fig. 7. Elements distribution in precipitations after tempering at 665 °C for3 h

Fig. 8 shows a sample area after tempering at 550 °C for 25 h, and Table 5 shows the elemental composition of precipitates and matrix. In all small dark precipitates (No. 1–3, 5, 6), a large amount of chromium with the presence of matrix iron, as well as small amount of molybdenum, niobium and tungsten, is determined. In the matrix (No. 4), iron predominates with the presence of chromium and molybdenum. Carbide-forming

elements niobium and tungsten are not found in the matrix, because they diffuse to precipitates.

Let us refer to Table 2, which shows the average dimensions (d), density (ρ), and volume content (V) of carbides at different tempering regimes. In all samples, the density of $M_{23}C_6$ particles is 1.5–2 orders of magnitude higher than the density of NbC precipitates, and the size is three times smaller. Comparison of various tempering regimes with each other leads to the conclusion that the size of $M_{23}C_6$ carbides increases from 85 to 135 nm with an increase in the tempering temperature from 550 to 720 °C, and their density decreases from $8.8 \cdot 10^{19}$ to $4 \cdot 10^{19}$ m^{-3}. Apparently, this can be explained by the combined action of diffusion processes of dissolution and fusion of carbides.

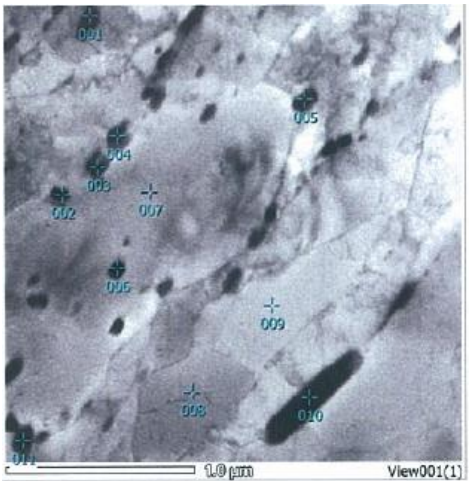

Fig. 8. Carbide precipitates in a sample after tempering at 550 °C for 25 h

Table 5

Elements distribution in a sample after tempering at 550°C for 25 h

No	at.%								
	C	Si	V	Cr	Mn	Fe	Nb	Mo	W
1	59.56	0.74	0.00	13.13	0.00	25.36	0.06	1.15	0.00
2	50.50	0.45	0.00	26.07	0.18	20.66	0.16	1.43	0.56
3	50.27	0.89	0.00	20.08	0.00	27.14	0.29	1.12	0.22
4	0.00	1.10	0.13	12.77	0.00	85.42	0.00	0.58	0.00
5	56.83	1.18	0.00	25.59	0.10	14.61	0.31	1.15	0.23
6	51.05	1.23	0.00	28.34	0.44	17.68	0.13	0.69	0.44
No	wt.%								
	C	Si	V	Cr	Mn	Fe	Nb	Mo	W
1	24.24	0.70	0.00	23.13	0.00	47.99	0.18	3.75	0.00
2	17.88	0.37	0.00	39.94	0.28	34.01	0.45	4.05	3.02
3	17.95	0.74	0.00	31.04	0.00	45.06	0.80	3.18	1.22
4		0.56	0.12	12.01	0.00	86.30	0.00	1.01	0.00
5	22.38	1.09	0.00	43.63	0.17	26.76	0.94	3.61	1.41
6	18.63	1.05	0.00	44.78	0.74	30.00	0.37	2.00	2.44

2.2. MECHANICAL PROPERTIES

The obtained experimental loading curves made it possible to calculate the characteristics of strength (σ_0, the proportionality limit, σ_b, the ultimate tensile strength) and plasticity (δ, the rupture elongation) of the specimens under study.

The final results of examining samples for uniaxial tension are shown in Fig. 9, as well as in Table 6; the latter also contains data on the microhardness of the samples. These results indicate the following:

1) the strength characteristics of materials decrease monotonically as the test temperature rises (see Fig. 9,a,b);

2) upsetting led to an increase in steel strength characteristics relative to their values for EI993+TT steel in the range from ~ 10 to ~ 60%, depending on the test temperature;

3) tempering after ausforming led to a drop in the values of σ_0 and σ_b in the entire temperature range of research, but nevertheless these characteristics remained predominantly higher than in steel EI993+TT;

4) the relative elongation of the sample after rupture, δ, in steel after ausforming decreases relative to the values in standard steel (see Fig. 9,c);

5) tempering increases the δ values, and at high test temperatures they exceed those in the standard steel.

For greater clarity and the possibility of comparison with the GOST indicators, the experimental results on the mechanical properties of steel are presented in the temperature range above 0°C (see Fig. 10). Fig. 10 demonstrates a good compliance of the strength parameters of standard steel with the GOST conditions, as mentioned earlier. Somewhat worse agreement is observed for plasticity.

Fig. 10 illustrates well the effect of upsetting (ausforming) and subsequent tempering on the mechanical characteristics of steel. It can be seen that these characteristics exceed the requirements of GOST in terms of strength indicators at all temperatures, including the region of high operating temperatures. The plasticity of the studied samples in the range of operating temperatures remains either at the level of GOST requirements, or slightly decreases from them.

Table 6

Mechanical characteristics of samples of the 12CrWMoNbVB steel in different states and at different test temperatures

State			EI993+TT	Upsetting	Upsetting+ tempering 720 °C for 3 h	Upsetting+ tempering 665 °C for 3 h	Upsetting+ tempering 550 °C for 25 h
H_μ, MPa			262	370	280	305	317
σ_0, MPa	T, °C	-196	1240	1420	1280	1270	1390
		20	680	1040	800	830	840
		550	420	680	540	520	420
		650	280	340	260	345	400
σ_b, MPa	T, °C	-196	1370	1520	1390	1355	1480
		20	910	1170	950	990	1020
		550	540	840	580	575	650
		650	400	370	380	390	440
δ, %	T, °C	-196	10.4	7.3	13.6	–	9.5
		20	11.4	5	9.3	12.2	8.4
		550	>10	10	18.4	13.5	17.1
		650	–	18	22.3	19.5	26

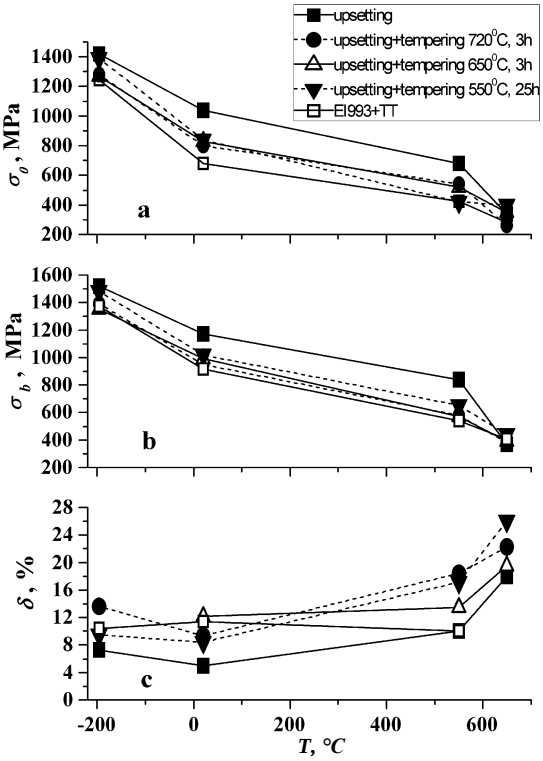

Fig. 9. Temperature dependences of the proportionality limit σ_0 (a), the ultimate strength σ_b (b), and the rupture elongation δ (c) of steel samples in different states

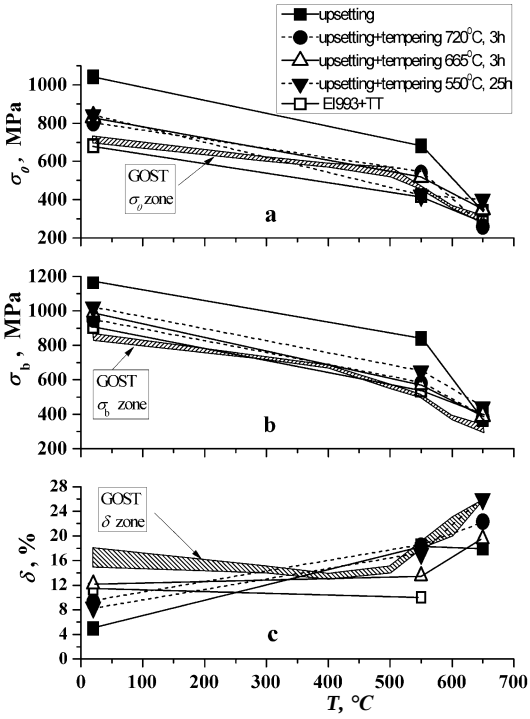

Fig. 10. Dependences of the proportionality limit σ_0 (a), the ultimate strength σ_b (b) and the rupture elongation δ (c) of steel samples in different states on the test temperature $T > 0$ °C and the area of the corresponding characteristics according to GOST (shaded zones)

The obtained experimental results on the mechanical properties (Figs. 9, 10, and Table 6) quite convincingly demonstrate that, among the three modes of heat treatment after ausforming, the best combination of mechanical properties is provided by tempering at 550 °C for 25 h.

Let us analyze the obtained results using the expression for the yield stress of an alloy according to the rule of mixtures:

$$\sigma_0 = \sigma_f + \sigma_{ss} + \sigma_d + \sigma_{cp} + \sigma_{gb}, \quad (1)$$

where σ_f is the stress caused by the friction of dislocations when moving in iron; σ_{ss} is solid solution hardening associated with interstitial and substitution atoms; σ_d is dislocation hardening; σ_{cp} is hardening due to precipitation of carbides, and σ_{gb} is grain boundary hardening. Due to the lack of the entire volume of necessary data, it is impossible to give a quantitative estimate of σ_0, but a qualitative assessment of the change in this characteristic can be made. Note that the values of σ_f and σ_{ss} are constant and are determined by the atomic structure of iron and chemical composition of the steel.

The dislocation density in the samples was not determined. The average size of subgrains in the samples after tempering is practically the same (see Table 2). Considering these factors, the analysis of formula (1) is reduced to the analysis of behavior of the "carbide" term σ_{cp}. As noted earlier, in the steel under study, the density of $M_{23}C_6$ precipitates is 1.5–2 orders of magnitude higher than the density of NbC precipitates, and the size is three times less (see Table 2). Consequently, all other things being equal, it is the $M_{23}C_6$ precipitates that should play a decisive role in the evolution of σ_0.

According to the model of dispersed barrier hardening [22],

$$\sigma_{cp} \sim (\rho d)^{1/2}, \quad (2)$$

where ρ is the density of precipitates (barriers), d is their average diameter. If we refer to Table 2, we can see that when tempering at 550 °C for 25 h, the highest density of carbide precipitates $M_{23}C_6$ ($\rho = 8.8 \cdot 10^{19}$ m^{-3}) with the smallest average diameter (d = 86 nm) is observed. Direct calculation by relation (2) gives the following values (aside from the dimension): 27, 27, and 22 for the tempering modes 550 °C, 25 h; 665 °C, 3 h, and 720 °C, 3 h, respectively. Taking into account the strong simplification of the assessment, these results can be considered to be quite strong evidence in favor of the 550 °C, 25 h tempering regime.

CONCLUSIONS

1. A complex of electron microscopic studies of steel was carried out, which provided information on the subgrain structure, type and parameters of precipitates in steel samples in different states. The main precipitates are carbides of the $M_{23}C_6$ and NbC types, and the density of the former is 1.5–2 orders of magnitude higher than that of the latter, depending on the state of the steel.

2. Tests for uniaxial tension of samples of the steel 12CrWMoNbVB, which underwent preliminary ausforming by upsetting at temperature of about 890 °C and subsequent tempering in three modes (720 °C for 3 h; 665 °C for 3 h; 550 °C for 25 h), were carried out. The samples were investigated at four temperatures: -196 (in liquid nitrogen); 20; 550, and 650°C (the last two tests were carried out in vacuum). Measurements of the microhardness of these samples at room temperature were also performed.

These studies made it possible to determine the characteristics of the strength and plasticity of steel samples in different states: the proportionality limit σ_0, the ultimate tensile strength σ_b, and the rupture elongation δ.

It has been established that ausforming and subsequent tempering provide an increase in σ_0 and σ_b of the steel relative to their values for the standard steel (according to GOST requirements) in the entire range of research temperatures. In this case, the ductility δ of the treated steel in the region of high operating temperatures also increases.

3. The best combination of mechanical properties, especially in the area of high operating temperatures, is achieved after tempering at 550 °C for 25 h. In this case, precipitates of carbides of the $M_{23}C_6$ type can play a significant role.

REFERENCES

1. R.L. Klueh, A.T. Nelson. Ferritic/martensitic steels for next-generation reactors // *Journal of Nuclear Materials*. 2007, N 37, p. 37-52.

2. V.N. Voyevodin, I.M. Neklyudov. Problems of radiation resistance of structural materials for nuclear power engineering // *Bulletin of Kharkov University*. 2006, N 746, p. 3-22.

3. T.N. Kompaniets. On the problem of choosing steels for the DEMO reactor // *Problems of Atomic Science and Technology. Series "Thermonuclear fusion"*. 2009, N 3, p. 16-24.

4. M.V. Leontieva-Smirnova et al. Microstructure and mechanical properties of low-activated ferritic-martensitic steel EK-181 (RUSFER-EK-181) // *Perspective materials*. 2006, N 6, p. 40-52.

5. M.V. Leontieva-Smirnova et al. Structural features of heat-resistant 12% chromium steels with a rapid decline in activity // *Problems of Atomic Science and Technology. Series "Materials Science and New Materials*. 2004, N 2(63), p. 142-155.

6. V.M. Chernov et al. Structural materials for fusion power reactors – the RF R&D activities // *Nuclear Fusion*. 2007, v. 47, p. 1-10.

7. Q. Huang et al. Recent progress of R&D activities on reduced activation ferritic/martensitic steels // *Journal of Nuclear Materials*. 2013, N 442, p. S2-S8.

8. R.L. Klueh, D.R. Harries. *High-chromium ferritic and martensitic steels for nuclear applications*. ASTM Stock Number MONO3, 2001, 221 p.

9. G.N. Ermolaev, I.V. Golikov, M.V. Leontieva-Smirnova, G.I. Melnikov, E.M. Mozhanov, V.M. Chernov. Mechanical properties of low-activated ferritic-martensitic 12% chromium steel EK181 (RUSFER-EK-181) under static and shock loads // *Problems of Atomic Science and Technology. Series "Materials Science and New Materials"*. 2006, N 2(67), p. 271-279.

10. V.M. Chernov, G.N. Ermolaev, M.V. Leontieva-Smirnova. Fracture toughness of chromium (12%) ferritic-martensitic steel EK-181 under loading on concentrated bending // *Journal of Technical Physics*. 2010, v. 80, issue 7, p. 72-77.

11. *Metallurgy and heat treatment of steel:* Reference book in 3 volumes / Ed. M.L. Bernstein and A.G. Rakhstadt. M.: "Metallurgiya", 1983, v. 3, 215 p.

12. G.T. Eldis, M. Cohen. Strength of Initially Virgin Martensites at –196 °C after Aging and Tempering // *Metall. Trans. A*. 1983, v. 14A, p. 1007-1012.

13. N.A. Polekhina, I.Yu. Litovchenko, A.N. Tyumentsev, D.A. Kravchenko, V.M. Chernov, M.V. Leontieva-Smirnova. Influence of high-temperature thermomechanical treatment in the austenitic region on the microstructure and mechanical properties of low-activated 12% chromium ferritic-martensitic steel EK-181 // *Journal of Technical Physics*. 2017, v. 87, issue 5, p. 716-721.

14. S. Hollner et al. High-temperature mechanical properties improvement on modified 9Cr-1Mo

martensitic steel through thermomechanical treatments // *Journal of Nuclear Materials*. 2010, N 367, p. 101-105.

15. L. Tan et al. Microstructure control for high strength 9% Cr ferritic-martensitic steels // *Journal of Nuclear Materials*. 2012, N 422, p. 45-50.

16. R.L. Klueh, N. Hashimoto, P.J. Maziasz. New nano-particle-strengthened ferritic/martensitic steels by conventional thermo-mechanical treatment // *Journal of Nuclear Materials*. 2007, N 367-370, p. 48-53.

17. S. Hollner et al. Characterization of a boron alloyed 9Cr3W3CoVNbBN steel and further improvement of its high-temperature mechanical properties by thermomechanical treatments // *Journal of Nuclear Materials*. 2013, N 441, p. 15-23.

18. *Brand of steels and alloys* / Ed. A.S. Zubchenko. M.: "Mechanical Engineering", 2003.

19. K.A. Lanskaya. *High-chromium heat-resistant steels*. M.: "Metallurgy", 1976, 216 p.

20. http://www.splav-kharkov.com/main.php

21. GOST 5949-75. *Graded and calibrated corrosion-resistant, heat-resistant and heat-resistant steel*. M.: "IPK Ed. Standards", 2004.

22. K. Cho, S. Park, D. Choi, H. Kwon. Influence of Ti addition on the microstructure and mechanical properties of a 5% Cr-Mo-V steel // *J. Alloys Compd*. 2015, v. 626, p. 314-322.

Article received 06.12.2021

ВЛИЯНИЕ АУСФОРМИНГА НА МЕХАНИЧЕСКИЕ СВОЙСТВА 12%Cr ФЕРРИТОМАРТЕНСИТНОЙ СТАЛИ

И.Ф. Кисляк, А.Ю. Ростова, Н.Ф. Андриевская, А.С. Кальченко, В.С. Оковит, М.А. Тихоновский, Р.Л. Василенко, И.Г. Танцюра, В.А. Панов

Исследовано влияние аусформинга путем осадки при 890 °С и последующего отпуска на микроструктуру и механические свойства при одноосном растяжении ферритомартенситной стали 12CrWMoNbVB (18Х12ВМБФР – по ГОСТ 5632-72). Электронно-микроскопические исследования, а также элементный анализ образцов стали в различных состояниях позволили получить подробную информацию о субзеренной структуре и типичных выделениях. Последние в основном представлены карбидами $M_{23}C_6$ и NbC. Исследованы параметры прочности и пластичности (σ_0, σ_b, δ), которые улучшаются при применяемой термомеханической обработке по сравнению со стандартными характеристиками стали. Предварительно оценивается предпочтительная обработка стали.

ВПЛИВ АУСФОРМІНГУ НА МЕХАНІЧНІ ВЛАСТИВОСТІ 12%Cr ФЕРИТОМАРТЕНСИТНОЇ СТАЛІ

І.П. Кісляк, Г.Ю. Ростова, Н.Ф. Андрієвська, О.С. Кальченко, В.С. Оковіт, М.А. Тихоновський, Р.Л. Василенко, І.Г. Танцюра, В.А. Панов

Досліджено вплив аусформінгу шляхом осаджування при 890 °С та подальшого відпускання на мікроструктуру і механічні властивості за одновісного розтягу феритомартенситної сталі 12CrWMoNbVB (18Х12ВМБФР – за ГОСТ 5632-72). Електронно-мікроскопічні дослідження, а також елементний аналіз зразків сталі в різних станах дозволили отримати детальну інформацію про субзеренну структуру та типові виділення. Останні переважно представлені карбідами $M_{23}C_6$ та NbC. Досліджено параметри міцності та пластичності (σ_0, σ_b, δ), котрі покращуються після застосованої обробки у порівнянні зі стандартними характеристиками сталі. Попередньо оцінено переважну обробку сталі.